Atomic Proximity between S4 Segment and Pore Domain in Shaker Potassium Channels

Muriel Lainé,[1,4] Meng-chin A. Lin,[1]
John P.A. Bannister,[1] William R. Silverman,[1,5]
Allan F. Mock,[1] Benoit Roux,[3]
and Diane M. Papazian[1,2,*]
[1]Department of Physiology and
[2]Molecular Biology Institute
David Geffen School of Medicine
University of California, Los Angeles
Los Angeles, California 90095
[3]Department of Biochemistry
Weill Medical College of Cornell University
New York, New York 10021

Summary

A recently proposed model for voltage-dependent activation in K^{+} channels, largely influenced by the KvAP X-ray structure, suggests that S4 is located at the periphery of the channel and moves through the lipid bilayer upon depolarization. To investigate the physical distance between S4 and the pore domain in functional channels in a native membrane environment, we engineered pairs of cysteines, one each in S4 and the pore of Shaker channels, and identified two instances of spontaneous intersubunit disulfide bond formation, between R362C/A419C and R362C/F416C. After reduction, these cysteine pairs bound Cd^{2+} with high affinity, verifying that the residues are in atomic proximity. Molecular modeling based on the MthK structure revealed a single position for S4 that was consistent with our results and many other experimental constraints. The model predicts that S4 is located in the groove between pore domains from different subunits, rather than at the periphery of the protein.

Introduction

Voltage-dependent K^{+} channels contain two main functional modules: the voltage sensor and the pore. Changes in the transmembrane potential trigger conformational changes in the voltage sensor that regulate the probability of pore opening (reviewed by Bezanilla, 2000). During activation, the voltage sensor in each subunit undergoes at least two voltage-dependent conformational changes, resulting in a conformation that is permissive for pore opening (Bezanilla et al., 1994; Zagotta et al., 1994; Schoppa and Sigworth, 1998). Once all of the subunits are in this conformation, opening of the pore occurs cooperatively (Ledwell and Aldrich, 1999; Yifrach and MacKinnon, 2002).

Voltage-dependent K^{+} channels contain four subunits surrounding a central aqueous pore for K^{+} permeation

*Correspondence: papazian@mednet.ucla.edu
[4]Present address: Laboratory of Cardiac/Membrane Physiology, Rockefeller University, New York, New York 10021.
[5]Present address: Department of Molecular Biophysics and Biochemistry, Yale University, New Haven, Connecticut 06520.

(MacKinnon, 1991; Schulteis et al., 1996; Sokolova et al., 2001). Each subunit contains six transmembrane segments, S1–S6, and a reentrant P loop (Figure 1A). The first four transmembrane segments, S1–S4, constitute the voltage sensor domain. Charged residues in this module, primarily in S4, interact electrostatically with the transmembrane potential and initiate the conformational changes that control opening of the pore (Aggarwal and MacKinnon, 1996; Seoh et al., 1996). The pore of the channel is formed by the last two transmembrane segments, S5 and S6, and the P loop, which lines the narrowest part of the pore and confers selectivity for K^{+} over other cations (MacKinnon and Yellen, 1990; Yellen et al., 1991; Heginbotham et al., 1992; Doyle et al., 1998).

A large body of work has contributed to a model of voltage-dependent activation in which the highly charged S4 is a transmembrane segment shielded by other parts of the protein from direct contact with the lipid environment; upon depolarization, the S4 segment transfers several of its charged side chains between solvent-accessible locations on opposite sides of the membrane (reviewed by Bezanilla 2000, 2002; Gandhi and Isacoff, 2002; Horn, 2002). Recently, however, this model has been seriously challenged by the X-ray structure of a voltage-dependent K^{+} channel, KvAP, from the hyperthermophilic archaebacterium *Aeropyrum pernix* (Jiang et al., 2003a). The KvAP structure contains several unexpected and surprising features. One of these is an intracellular location for the S4 segment (Jiang et al., 2003a). Largely influenced by this structure, MacKinnon and coworkers have proposed an alternative model for voltage-dependent activation in which the positively charged S4 is located at the periphery of the channel protein and moves through the hydrophobic lipid environment during activation (Jiang et al., 2003b). This model seemingly contradicts a wide variety of previously reported data (Larsson et al., 1996; Yusaf et al., 1996; Starace et al., 1997; Cha et al., 1999; Blaustein et al., 2000; Elinder et al., 2001; Starace and Bezanilla, 2001). Thus, an important question is whether the structure of KvAP reflects a functionally relevant conformation despite detergent solubilization and complexation with a monoclonal Fab fragment. A key issue in this debate is the location of the S4 segment relative to the pore domain in a functional voltage-dependent channel protein located in a native membrane.

We have now tested the hypothesis that S4 in the voltage sensor interacts directly with the pore in K^{+} channels. We have identified residues in S4 and the pore domain that come within atomic distance of each other during activation of the voltage-dependent Shaker channel. Using the structure of the MthK channel as a reasonable model for the pore domain of Shaker in the open conformation, we have developed a structural model for interactions between the voltage sensor and the pore using a molecular dynamics simulated annealing procedure. Our data support a dramatically different view of voltage sensor/pore interactions than that pro-
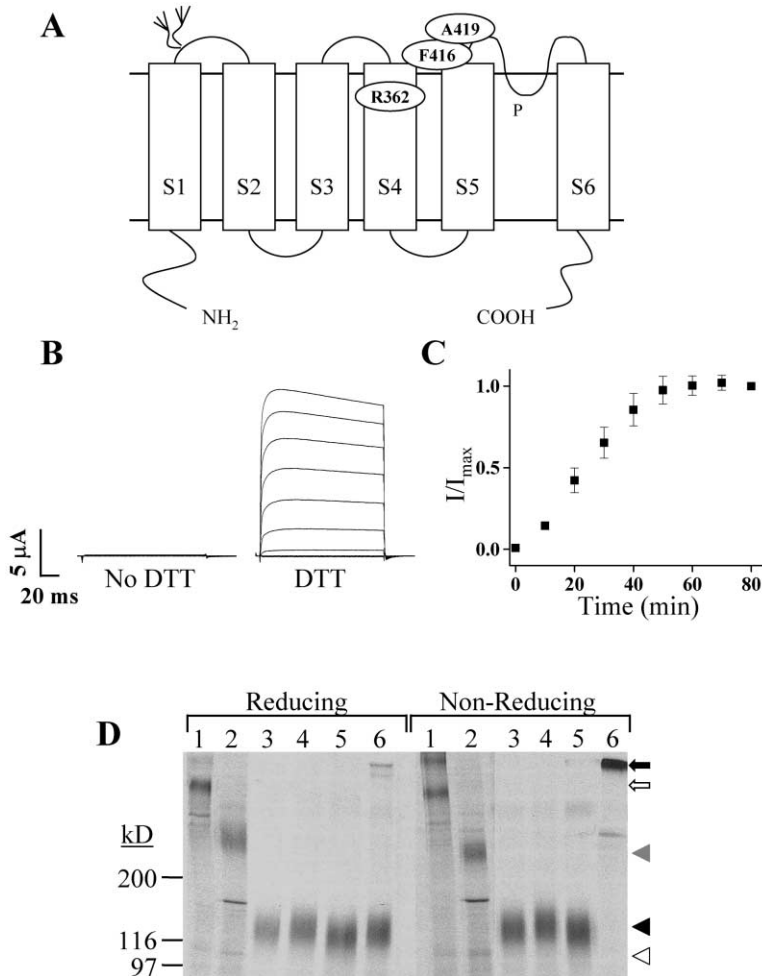
Figure 1. R362C and A419C Spontaneously Form an Intersubunit Disulfide Bond

(A) A model for the membrane topology of the Shaker subunit is shown. Transmembrane segments S1 through S6 and the reentrant P loop have been labeled. The approximate positions of R362, F416, and A419 are also shown.

(B) Current traces from an oocyte expressing R362C + A419C channels were recorded before and after a 30 min treatment with 5 mM DTT. A representative experiment is shown (n = 6). The membrane potential was stepped from a holding potential of −100 mV to potentials between −100 and +60 mV in 20 mV increments.

(C) Current amplitudes at +40 mV were measured after various times of incubation in 5 mM DTT. Current amplitudes were normalized to the current level after 80 min incubation (I/I_{max}) (n = 4).

(D) Shaker protein was metabolically labeled, isolated, and subjected to electrophoresis under reducing or nonreducing conditions, as indicated. Lanes 1 through 6 contain (1) a covalent tetramer of Shaker subunits; (2) a covalent dimer of Shaker subunits; (3) Shaker-IR; (4) R362C single mutant; (5) A419C single mutant; and (6) R362C + A419C double mutant. A fluorograph of a representative experiment is shown (n = 4). Oocytes were treated with 5 mM NEM prior to disruption, except for cells expressing the covalent tetramer, which were treated with 0.1% H_2O_2 for 15 min at room temperature to oxidize intersubunit disulfide bonds between two cytoplasmic cysteine residues, C96 and C505, prior to NEM treatment (Schulteis et al., 1996). Under nonreducing conditions, the R362C + A419C protein comigrated with the disulfide-bonded circular tetramer (black arrow). The open arrow indicates the position of the linear tetramer under reducing conditions. The gray and black arrowheads denote the positions of the complex glycosylated dimeric and monomeric Shaker proteins, respectively (Nagaya and Papazian, 1997). The white arrowhead indicates the position of the immature, core-glycosylated form of the Shaker protein. All of the constructs matured efficiently, making the immature form virtually undetectable.

posed by MacKinnon and coworkers on the basis of the KvAP structure (Jiang et al., 2003a; 2003b).

Results

Spontaneous Intersubunit Disulfide Bond Forms between R362C and A419C

To test the hypothesis that S4 interacts directly with the pore domain in voltage-gated K⁺ channels, we paired cysteine mutations, one each in S4 and the pore domain of the Shaker channel, to identify instances of spontaneous disulfide bond formation. The vast majority of double cysteine mutants (17 out of 19 functional constructs) provided no evidence for disulfide bond formation (see Figure 8). One exception was the double mutant R362C + A419C (Figure 1A). The R362C + A419C construct generated no currents in *Xenopus* oocytes unless the cells were first incubated with the reducing agent DTT (Figure 1B). Upon exposure to DTT, current amplitude increased after a short lag, reaching a maximum after approximately 50 min (Figure 1C). These results suggest that R362C and A419C form a disulfide bond.

Biochemical analysis confirmed that R362C and A419C spontaneously form a disulfide bond and revealed that the reaction occurs between residues in adjacent subunits rather than in the same subunit (Figure 1D). The Shaker-IR, R362C, A419C, and R362C + A419C proteins were metabolically labeled with [³⁵S]methionine in oocytes. Forty-eight hours after injection, oocytes were treated with N-ethylmaleimide to protect free sulfhydryl groups and then were extracted with detergent. Solubilized Shaker protein was immunoprecipitated and subjected to electrophoresis under reducing and nonreducing conditions. Each of the Shaker proteins matured efficiently to the complex glycosylated form, a reliable indication that they had folded and assembled properly (Figure 1D) (Papazian et al., 1995; Nagaya and Papazian, 1997; Tiwari-Woodruff et al., 1997; Schulteis et al., 1998). The Shaker-IR protein and the single mutants R362C and A419C were detected as monomers under both reducing and nonreducing conditions (Figure 1D) (Santacruz-Toloza et al., 1994; Nagaya and Papazian, 1997). In contrast, the double mutant R362C + A419C protein migrated as a monomer only under reducing conditions.
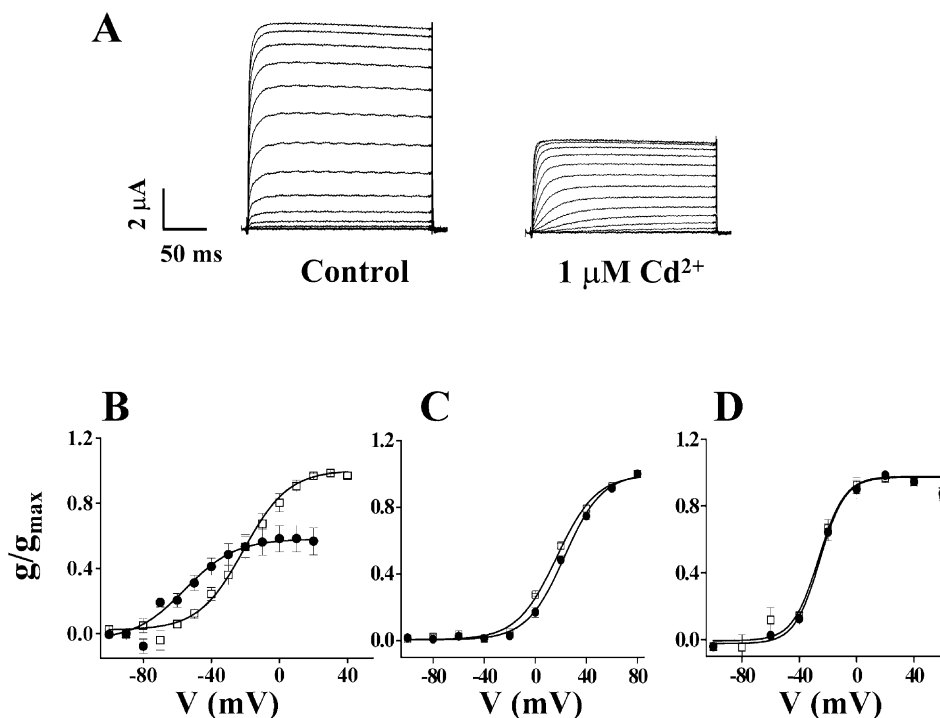
Figure 2. After Reduction, C362 and C419 Form a Cd^{2+} Binding Site

(A) Oocytes expressing R362C + A419C channels were incubated in 2 mM DTT for 90 min and washed extensively. Current traces were recorded in the presence or absence of 1 μM Cd^{2+}, as indicated. A representative experiment is shown (n = 8). The membrane potential was stepped from a holding potential of –100 mV to potentials between –100 and +60 mV in 10 mV increments. Cd^{2+} reduced the current amplitude, measured at +40 mV, to 47% of its original value (6.9 ± 0.7 μA compared to 14.5 ± 1.0 μA, n = 8).

(B–D) Normalized conductance-voltage (g-V) curves obtained in the absence (open squares) or presence (closed circles) of 1 μM Cd^{2+} for (B) R362C + A419C, (C) R362C, and (D) A419C channels are shown. Conductance (g) values obtained in either the presence or absence of Cd^{2+} were normalized to the maximal g value obtained in the absence of Cd^{2+} in the same experiment. For the R362C and A419C single mutants, Cd^{2+} had no significant effect on current amplitude. As a result, the maximal g values obtained in the presence and absence of Cd^{2+} were the same. Values are shown as mean ± SEM, n = 4–6. Each data set was fitted with a single Boltzmann function (solid curves). The fitted parameters in the absence of Cd^{2+} were as follows: R362C + A419C, $V_{1/2}$ = −24.4 ± 1.1 mV and slope = 19.1 ± 0.8 mV; R362C, $V_{1/2}$ = 16.7 ± 1.8 mV and slope = 15.4 ± 1.6 mV; A419C, $V_{1/2}$ = −28.0 ± 3.2 mV and slope = 8.5 ± 1.0 mV. The fitted parameters in the presence of 1 μM Cd^{2+} were R362C + A419C, $V_{1/2}$ = −55.9 ± 3.2 mV and slope = 14.3 ± 2.4 mV; R362C, $V_{1/2}$ = 22.7 ± 1.4 mV and slope = 14.7 ± 1.2 mV; A419C, $V_{1/2}$ = −27.2 ± 3.0 mV and slope = 8.6 ± 2.1 mV.

Under nonreducing conditions, the R362C + A419C protein migrated as a high molecular weight adduct close to the position expected for a tetramer of Shaker subunits (Figure 1D). These results indicate that C362 in S4 and C419 in the pore domain spontaneously form an intersubunit disulfide bond.

To confirm that the disulfide-bonded adduct of R362C + A419C subunits corresponds to a tetramer, we compared its mobility to that of authentic covalently linked dimers and tetramers of Shaker subunits (Figure 1D). The disulfide-bonded R362C + A419C protein migrated in the vicinity of the covalent tetramer, a linear molecule. We have previously shown that linear and closed circular tetramers of Shaker subunits have slightly different electrophoretic mobilities (Schulteis et al., 1996). To form a size marker for a closed circular tetramer of Shaker subunits, cells expressing the covalent tetramer were exposed to mild oxidizing conditions. The Shaker protein contains two cytoplasmic cysteine residues, C96 and C505, which form an intersubunit disulfide bond under oxidizing conditions (Schulteis et al., 1996). This bond does not form spontaneously in

intact cells, because the cysteine residues are located in the reducing environment of the cytoplasm (Figure 1D) (Schulteis et al., 1996). Significantly, the disulfide-bonded R362C + A419C adduct comigrated under nonreducing conditions with the closed circular tetramer formed by oxidation of the C96/C505 disulfide bond in the covalent tetramer. These results indicate that the R362C + A419C protein contains four intersubunit disulfide bonds that form spontaneously and efficiently in intact cells.

After Reduction, a High-Affinity Cd^{2+} Binding Site Is Formed by R362C and A419C

Formation of a disulfide bond between R362C in S4 and A419C in the pore domain suggests that these residues are in physical proximity. However, in flexible proteins, cysteine residues normally separated by as much as 15 Å may be able to form disulfide bonds during visits to rare conformations (Careaga and Falke, 1992). Therefore, we investigated whether C362 and C419 are able to form a high-affinity Cd^{2+} binding site, in which Cd^{2+} interacts simultaneously with both cysteine residues.
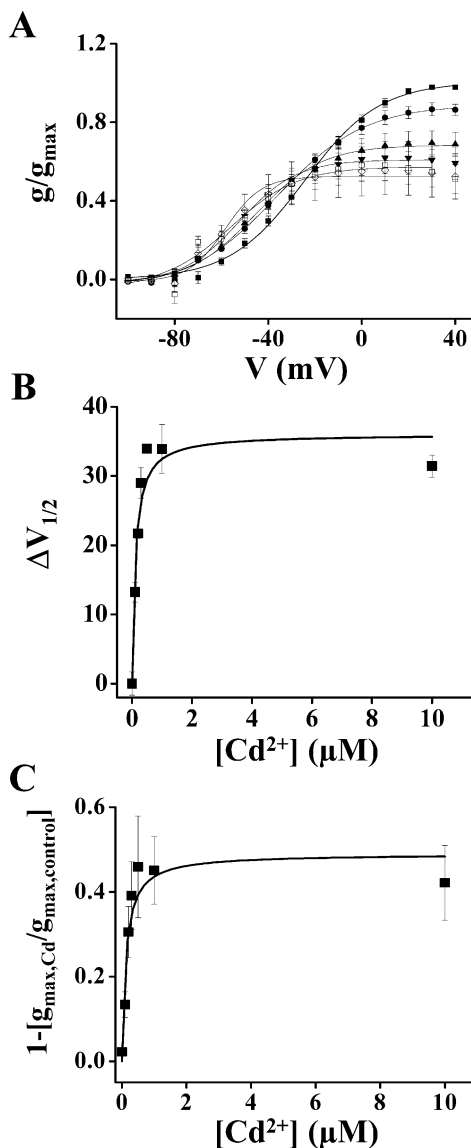
Figure 3. After Reduction, R362C + A419C Binds Cd^{2+} with High Affinity

(A) Normalized g-V curves for R362C + A419C channels were obtained in the absence (closed squares) or presence of 0.1 μM (black circles), 0.2 μM (black triangles), 0.3 μM (black inverted triangles), 0.5 μM (open diamonds), and 1 μM (open squares) Cd^{2+} (n = 3–6). Conductance (g) values obtained in either the presence or absence of Cd^{2+} were normalized to the maximal g value obtained in the absence of Cd^{2+} in the same experiment. A Boltzmann function was fitted to each data set (solid curves). The fitted parameters were as follows: no Cd^{2+}, $V_{1/2}$ = −24.4 ± 1.1 mV and slope = 19.1 ± 0.8 mV; 0.1 μM Cd^{2+}, $V_{1/2}$ = −36.9 ± 1.2 mV and slope = 18.6 ± 1.0 mV; 0.2 μM Cd^{2+}, $V_{1/2}$ = −45.5 ± 2.0 mV and slope = 14.5 ± 2.0 mV; 0.3 μM Cd^{2+}, $V_{1/2}$ = −52.3 ± 2.1 mV and slope = 12.2 ± 1.7 mV; 0.5 μM Cd^{2+}, $V_{1/2}$ = −58.4 ± 2.8 mV and slope = 7.8 ± 2.0 mV; and 1.0 μM Cd^{2+}, $V_{1/2}$ = −55.9 ± 3.2 mV and slope 14.3 ± 2.4.

(B) A plot of $\Delta V_{1/2}$ versus Cd^{2+} concentration is shown. $\Delta V_{1/2}$ is the difference between the fitted $V_{1/2}$ values obtained in the absence and presence of Cd^{2+}. The data were fitted with a hyperbolic function (solid curve) with a half-maximal concentration of 0.11 ± 0.04 μM. Values are shown as mean ± SEM, n = 3–6.

(C) A plot of the fractional decline in maximal conductance in the presence of Cd^{2+}, 1 − [$g_{max,Cd}/g_{max,control}$], versus Cd^{2+} concentration

After reduction with DTT, the functional properties of R362C + A419C were compared in the presence and absence of 1 μM Cd^{2+} (Figure 2). Treatment with Cd^{2+} decreased the current amplitude and shifted the voltage dependence of activation in the hyperpolarized direction (Figures 2A and 2B). These functional effects were completely reversed after perfusion with a bath solution containing 1 mM EGTA (data not shown). In contrast, Cd^{2+} did not affect the current amplitude (data not shown) or shift the conductance versus voltage (g-V) curve of the R362C or A419C single mutants (Figures 2C and 2D). Cd^{2+} also had no effect on the control channel Shaker-IR (data not shown).

To estimate the Cd^{2+} affinity of the R362C + A419C double mutant, the voltage dependence of activation was determined at different Cd^{2+} concentrations (Figure 3A). Increasing the Cd^{2+} concentration from 0.1 to 1 μM resulted in a progressive shift of the g-V curve in the hyperpolarized direction. The g-V curve obtained at each concentration was fitted with a single Boltzmann function to obtain a midpoint voltage, $V_{1/2}$. The difference in $V_{1/2}$ measured in the presence and absence of Cd^{2+} ($\Delta V_{1/2}$) was plotted versus Cd^{2+} concentration (Figure 3B). These data were well fitted by a rectangular hyperbola, which indicated that the half-maximal effective Cd^{2+} concentration was approximately 110 nM.

To determine whether Cd^{2+} decreased the current amplitude with a similar apparent affinity, the fractional decline in maximum conductance (1 − [$g_{max,Cd}/g_{max,control}$]) was plotted versus Cd^{2+} concentration (Figure 3C). The data were fitted with a rectangular hyperbola, which indicated that the half-maximal effective Cd^{2+} concentration was approximately 120 nM (Figure 3C). Thus, Cd^{2+} shifted the voltage dependence of activation and decreased the current amplitude with the same apparent affinity within experimental error (see Figure 3 legend). This high affinity is consistent with the conclusion that the Cd^{2+} ion binds simultaneously to R362C and A419C, confirming that they are within atomic distance of each other (Yellen et al., 1994; Liu et al., 1997; Holmgren et al., 1998; Yamagishi et al., 1997; Loussouarn et al., 2001). Typically, $C\beta$ atoms in cysteine residues bridged by a Cd^{2+} ion are separated by 5–6 Å (Castagnetto et al., 2002).

Metal Ion Binding to R362H + A419H Stabilizes Activated Conformation

Bis-histidine residues form metal chelation sites that can be useful for probing structural interactions in membrane proteins (Jung et al., 1995; Norregaard et al., 2000; MacAulay et al., 2001). To explore further the proximity between positions 362 and 419, we generated the R362H + A419H double mutant and the R362H and A419H single mutants and examined the functional effects of Zn^{2+} (Figure 4A) and Cd^{2+} (data not shown). Application of 1 μM Zn^{2+} to R362H + A419H channels shifted the midpoint of the g-V curve by approxi-

is shown. The data were fitted with a hyperbolic function (solid curve) with a half-maximal concentration of 0.12 ± 0.05 μM. Values are shown as mean ± SEM, n = 3–6.
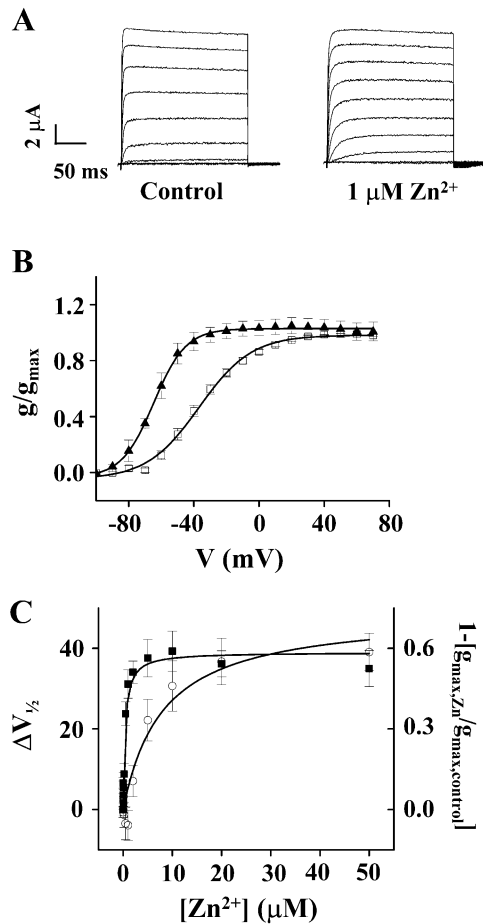
A

B

C

Figure 4. Zn^{2+} Binding to R362H + A419H Stabilizes an Activated Conformation of Shaker

(A) Currents from R362H + A419H channels were recorded in the presence or absence of 1 μM Zn^{2+}, as indicated. A representative experiment is shown, n = 9. The membrane potential was stepped from a holding potential of -100 mV to potentials between -100 and $+60$ mV in 20 mV increments.

(B) Normalized g-V curves for R362H + A419H channels were obtained in the absence (open squares) or presence (black triangles) of 1 μM Zn^{2+}. Conductance (g) values obtained in either the presence or absence of Zn^{2+} were normalized to the maximal g value obtained in the absence of Zn^{2+} in the same experiment. Each data set was fitted with a single Boltzmann function (solid curves). The fitted parameters obtained in the absence of Zn^{2+} were $V_{1/2} = -37.0 \pm 2.1$ mV and slope = 14.5 ± 0.6 mV, n = 18. The fitted parameters obtained in the presence of 1 μM Zn^{2+} were $V_{1/2} = -64.6 \pm 2.9$ mV and slope = 9.0 ± 0.5 mV, n = 8.

(C) Dose response curves for the two functional effects of Zn^{2+}, the shift in the g-V curve ($\Delta V_{1/2}$, filled squares) and the fractional decrease in maximal conductance ($1 - [g_{max,Zn}/g_{max,control}]$, open circles), are shown. Each data set was fitted with a hyperbolic function (solid curves). The half-maximal effective concentrations were $\Delta V_{1/2}$, 0.40 ± 0.07 μM, n = 6–10; $1 - [g_{max,Zn}/g_{max,control}]$, 8.0 ± 1.2 μM, n = 6–10. Values are shown as mean $\pm$ SEM.

mately -40 mV (Figure 4B). The Zn^{2+}-induced shift was the same direction and similar in amplitude to the shift caused by Cd^{2+} in R362C + A419C channels. In contrast, Zn^{2+} had no effect on the R362H or A419H single mutants (data not shown). Similarly to Zn^{2+}, Cd^{2+} left shifted the g-V curve of R362H + A419H but not R362H or A419H (data not shown).

To estimate the Zn^{2+} affinity of the double histidine mutant, the voltage dependence of activation was determined at different Zn^{2+} concentrations. $\Delta V_{1/2}$ values were plotted versus Zn^{2+} concentration (Figure 4C). The data were well fitted by a rectangular hyperbola, which indicated that the half-maximal effective Zn^{2+} concentration was approximately 400 nM. This high apparent affinity is consistent with the conclusion that the Zn^{2+} ion binds simultaneously to R362H and A419H, confirming once again that these positions are within atomic distance of each other (Keifer and Fierke, 1994; Loland et al., 1999; Norregaard et al., 2000). For comparison, the apparent affinities of Zn^{2+} binding sites formed by two histidine residues in the active site of the enzyme carbonic anhydrase II range from 100 nM to 1 μM (Keifer and Fierke, 1994).

At concentrations higher than 1 μM, Zn^{2+} decreased the amplitude of R362H + A419H currents (data not shown). To estimate the Zn^{2+} affinity for this effect, the fractional decline in maximum conductance ($1 - [g_{max,Zn}/g_{max,control}]$) was plotted versus Zn^{2+} concentration (Figure 4C). The data were fitted with a rectangular hyperbola, which indicated that the half-maximal effective concentration for the decrease in current amplitude was approximately 8.0 μM, which is 20-fold higher than that required to shift the g-V curve (Figure 4C). Since high concentrations of Zn^{2+} (1 mM) had no significant effect on the current amplitude of Shaker-IR, R362H, or A419H channels (data not shown), it is unlikely that the Shaker protein contains a second metal ion binding site that mediates this lower affinity action. A more plausible explanation is that the decline in current amplitude in the double histidine mutant has a different stoichiometry than the shift in the voltage dependence of activation and requires a greater number of ions bound per tetrameric channel.

To confirm that the bis-histidine metal ion binding site is formed at the interface between two subunits, similar to the disulfide bond between R362C and A419C, we coexpressed the R362H and A419H single mutant subunits and determined the effect of 1 μM Zn^{2+} on the g-V curve (Figure 5A). Addition of Zn^{2+} resulted in a small but reproducible shift of the g-V curve in the hyperpolarized direction, confirming that the binding site is formed between histidine residues located in adjacent subunits (Figures 5B and 5C).

The leftward shift in the voltage dependence of activation suggests that ion binding to either R362C + A419C or R362H + A419H channels increased the relative stability of an activated conformation of the voltage sensor. Ion binding also decreased the current amplitude, an effect that may be due to the accumulation of slow inactivation, which is a common property of voltage-dependent K^+ channels including KvAP and Shaker (Choi et al., 1991; Baukrowitz and Yellen, 1995; Ruta et al., 2003).

Disulfide Bond Formation Stabilizes an Activated Conformation

R362C + A419C channels containing four disulfide bonds are in a nonconducting conformation (Figure 1). We tested the hypothesis that disulfide bond formation, like metal ion binding, stabilizes the voltage sensor in
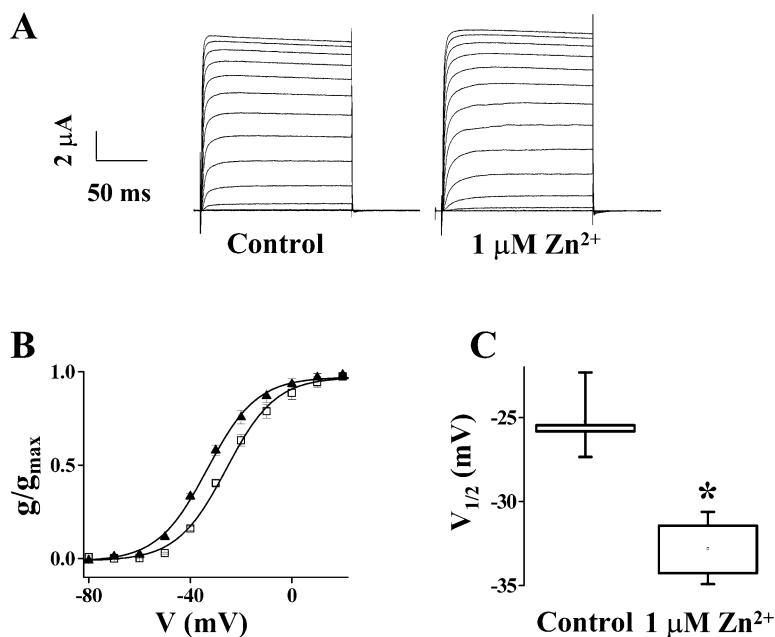
A

Control 1 μM Zn^{2+}

B

C

Control 1 μM Zn^{2+}

Figure 5. Zn^{2+} Binding Site Is Located at the Subunit Interface

(A) The R362H and A419H single mutants were coexpressed at a 1:1 cRNA ratio, and currents were recorded in the presence or absence 1 μM Zn^{2+}, as indicated. A representative experiment is shown, n = 4. The membrane potential was stepped from a holding potential of -100 mV to potentials between -100 and $+60$ mV in 10 mV increments.

(B) Normalized g-V curves of oocytes coexpressing R362H and A419H single mutants in the absence (open squares) or presence (closed triangles) of 1 μM Zn^{2+}. Each data set was fitted with a single Boltzmann function (solid curves). The fitted parameters were as follows: no Zn^{2+}, $V_{1/2} = -26.0 \pm 0.6$ mV and slope $= 9.6 \pm 0.5$ mV; with 1 μM Zn^{2+}, $V_{1/2} = -33.6 \pm 0.6$ mV and slope $= 9.5 \pm 0.5$ mV.

(C) Box plot of the $V_{1/2}$ values obtained in the absence and presence of 1 μM Zn^{2+} from oocytes coexpressing the R362H-IR and A419H-IR single mutants. Difference in $V_{1/2}$ values is statistically significant (one-way ANOVA, *p < 0.005, n = 4–11).

an activated conformation and results in the accumulation of slow inactivation. The voltage dependence of activation was monitored during acute reduction. During incubation with DTT, the g-V curve gradually shifted in the depolarized direction (Figure 6A). The shift was complete after approximately 50 min (Figure 6B) and therefore occurred over the same time period as the increase in current amplitude (Figure 1C). This result indicates that disulfide bond formation, like metal ion binding, is accompanied by a progressive shift of the g-V curve in the hyperpolarized direction. These results confirm that R362 and A419 are in proximity when the voltage sensor is in an activated conformation. In conjunction with ion binding or disulfide bond formation, the channel enters a nonconducting conformation, most likely due to the accumulation of slow inactivation.

R362C and F416C also Spontaneously Form an Intersubunit Disulfide Bond

The second instance of spontaneous disulfide bond formation occurred in the R362C + F416C double mutant. Expression of this construct in oocytes resulted in low channel activity. Current amplitudes were significantly increased by treatment with DTT (Figure 7A). Biochemical analysis revealed that R362C and F416C spontaneously form an intersubunit disulfide bond, similar to R362C and A419C (Figure 7B). After reduction of the disulfide bond, the functional properties of the R362C + F416C channel were compared in the presence and absence of Cd^{2+}. In contrast to the effect seen in R362C + A419C channels, Cd^{2+} shifted the g-V curve of R362C + F416C channels in the depolarized direction (Figure 7C). This result suggests that ion binding to R362C + F416C stabilizes the voltage sensor in a pre-open conformation. In addition, Cd^{2+} slowed the activation kinetics of R362C + F416C channels (Figure 7D). Slower kinetics were not due simply to the shift in the voltage depen-

dence of activation. At $+40$ mV, a potential where the open probability was maximal with or without Cd^{2+}, Cd^{2+} slowed activation (Figure 7D). In contrast, Cd^{2+} had no effect on the R362C or F416C single mutants (Figure 2B, data not shown).

The apparent affinity of Cd^{2+} binding was estimated by measuring the time to half-peak current amplitude as a function of Cd^{2+} concentration (Figure 7E). The half-maximal Cd^{2+} concentration was approximately 1.7 μM. A similar value, 1.2 μM, was obtained by plotting the change in activation midpoint as a function of Cd^{2+} concentration (data not shown). Although the apparent affinity for Cd^{2+} was about 10-fold lower in R362C + F416C than in R362C + A419C channels, it was within the range expected for simultaneous coordination by two cysteine residues (Yellen et al., 1994; Liu et al., 1997; Holmgren et al., 1998; Yamagishi et al., 1997; Loussouarn et al., 2001). However, the geometry or distance between R362C and F416C may be less optimal for Cd^{2+} binding than between R362C and A419C.

Proximity of R362 to A419 and F416 Is Specific

To verify that our results reflect specific structural proximity between R362 in S4 and A419 and F416 in the pore domain, we paired R362C with cysteine mutations of other pore residues to generate the R362C + A417C, R362C + V453C, and R362C + W454C double mutant constructs. Biochemical analysis indicated that intersubunit disulfide bonds do not form in these constructs (Figure 8A). After incubation in DTT, the functional properties of these double cysteine mutants were compared in the presence and absence of 1 μM Cd^{2+}. Cd^{2+} had no significant effects on current amplitude or the voltage dependence of activation (Figures 8B–8D). As expected, Cd^{2+} also had no effect on the functional properties of the A417C, V453C, and W454C single mutants (data not shown).
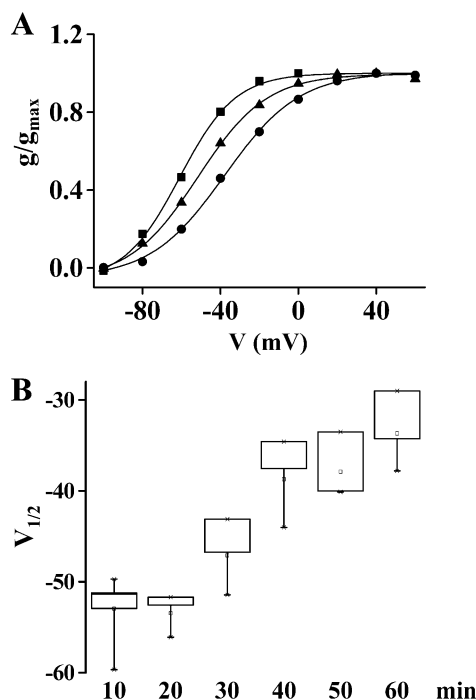
Figure 6. Acute Reduction of R362C + A419C Disulfide Bond Is Accompanied by Shift of g-V Curve in the Depolarized Direction

(A) Normalized g-V curves for R362C + A419C after 10 min (black squares), 30 min (black triangles), or 60 min (black circles) incubation in 5 mM DTT. Results of a representative experiment are shown, n = 3. Each data set was fitted with a single Boltzmann function (solid curves). Fitted parameters were as follows: 10 min, $V_{1/2} = -60.9 \pm 1.9$ mV and slope $= 14.3 \pm 1.7$ mV; 30 min, $V_{1/2} = -51.6 \pm 1.4$ mV and slope $= 17.6 \pm 1.6$ min; 60 min, $V_{1/2} = -37.8 \pm 1.37$ mV and slope $= 19.1 \pm 1.2$ mV.

(B) Box plot showing $V_{1/2}$ values obtained after different times of incubation in 5 mM DTT, n = 3–5.

Discussion

S4 Interacts Directly with Pore Domain

Our results provide compelling evidence that S4, the major functional element in the voltage sensor, interacts directly with the pore domain in voltage-dependent K^+ channels. We have investigated the physical proximity between R362 in the S4 segment and A419 in the pore domain of Shaker channels using three parallel approaches: disulfide bond formation, formation of a metal ion binding site by pairs of cysteine residues, and formation of a metal ion binding site by bis-histidine residues. Ion binding and disulfide bond formation had similar functional consequences and resulted in a consistent estimate of physical proximity. Our results were obtained with properly folded and assembled Shaker protein in a functional state in a native cellular membrane. The physical proximity that we detected was specific. Only 2 out of 19 functional cysteine pairs between likely solvent-accessible residues in S4 and the pore domain showed any evidence of disulfide bond formation or high-affinity Cd^{2+} binding after DTT treatment. Therefore, our results are not readily explained by the notion that a flexible voltage sensor is able to make random

contact with distant domains in the protein. Our data strongly suggest that voltage sensor/pore interactions in a native membrane are dramatically different than in the KvAP X-ray structure, obtained after detergent solubilization and complexation with a Fab fragment (Jiang et al., 2003a). Furthermore, it is difficult to reconcile our results with the model for voltage-dependent activation proposed by MacKinnon and coworkers, in which S4 is located at the periphery of the channel protein, 30–40 Å away from the pore domain, and moves through the hydrophobic lipid environment during activation (Jiang et al., 2003b).

Rather, our results indicate that R362, the first positively charged residue in the S4 segment, moves into atomic proximity of A419 during voltage-dependent activation of the Shaker channel. A419 corresponds to R52 in KcsA, a residue that maps to the perimeter of the pore domain, and is expected to be near the extracellular surface of the membrane (Doyle et al., 1998; Bernèche and Roux, 2000). Atomic proximity between R362 in S4 and A419 in the pore domain is supported by several observations. First, cysteine residues substituted at positions 362 and 419 efficiently and spontaneously formed disulfide bonds. These disulfide bonds were not due to the cytoplasmic cysteine residues C96 and C505, which do not react spontaneously (Schulteis et al., 1996). Consistent with this conclusion, we did not detect spontaneous disulfide bond formation in the Shaker-IR protein or in the single cysteine mutants. Second, after reduction, R362C and A419C bound Cd^{2+} with extremely high apparent affinity, consistent with the conclusion that two cysteine residues simultaneously coordinate the ion. Third, histidine residues substituted at these positions also generated a high-affinity metal ion binding site. Analysis of high-resolution protein structures indicates that disulfide bonds and cadmium- or zinc-mediated bridges are established only when the residues involved are in close physical proximity. The distance between $C\beta$ atoms in two disulfide-bonded residues is about 4 Å, whereas the $C\beta$ distance varies from 4.2 to 6.5 Å for two cysteines bridged by a Cd^{2+} ion or two histidines bridged by a Zn^{2+} ion (Alberts et al., 1998; Harding, 2001; Castagnetto et al., 2002; see also the Metalloprotein Database (MDB) at Scripps, http://metallo. scripps.edu). Therefore, despite differences in local chemical details, the disulfide bonds and the metal bridges represent relatively small variations in the interresidue distances, providing a consistent picture of the atomic level proximity between these positions.

We found that R362C was also able to form a disulfide bond and a metal ion binding site with F416C. F416 corresponds to L49 in KcsA. On the basis of the KcsA structure, the β carbon of F416 is expected to be located within 6 Å of the β carbon of A419. Interestingly, R362C + F416C channels had a 10-fold lower apparent affinity for Cd^{2+} than R362C + A419C channels. Thus, the precise orientation of the S4 residue relative to the pore domain can have a significant effect on the apparent affinity of the ion binding site. Furthermore, the functional effects of Cd^{2+} binding differed from those seen in the R362C + A419C channel. These results suggest the existence of a well-defined interaction surface between the voltage sensor and the pore where small changes in structure
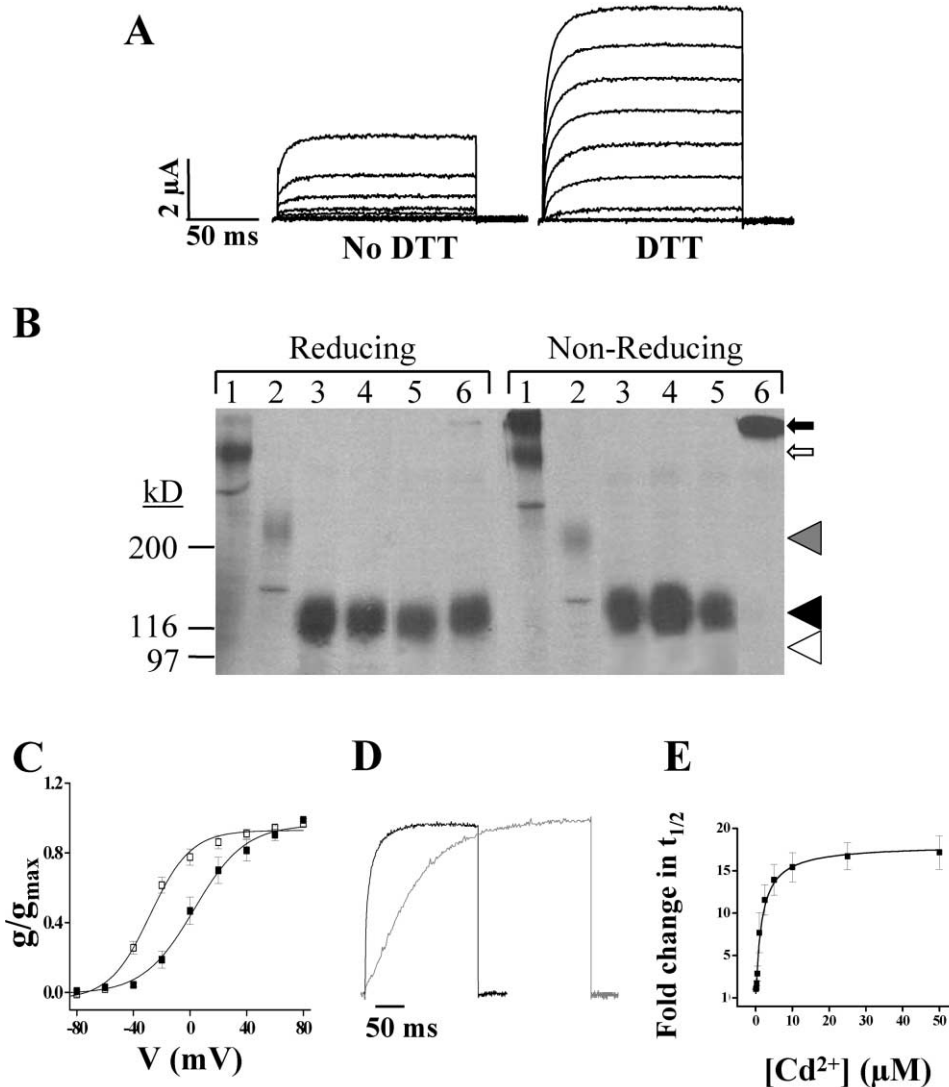
Figure 7. R362C and F416C also Spontaneously Form an Intersubunit Disulfide Bond and, after Reduction, Form a Cd²⁺ Binding Site
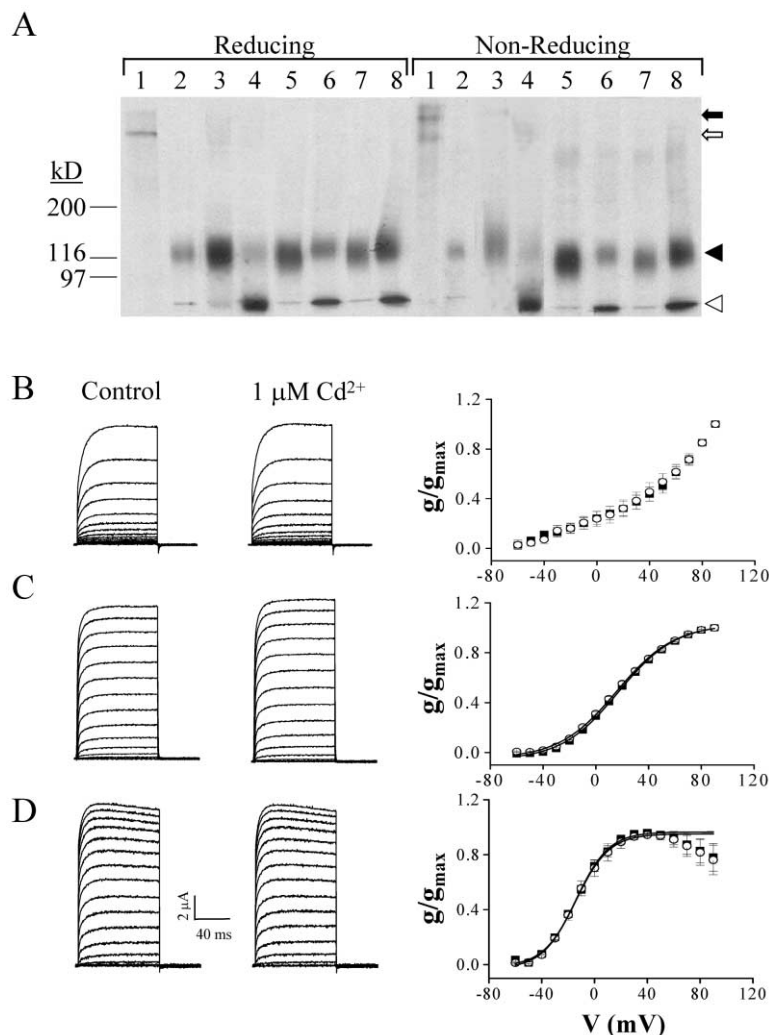
(A) Current traces from an oocyte expressing R362C + F416C channels were recorded before and after a 1 hr treatment with 2 mM DTT. A representative experiment is shown (n = 22). The membrane potential was stepped from a holding potential of –100 mV to potentials between –100 and +80 mV in 20 mV increments.

(B) Shaker protein was metabolically labeled, isolated, and subjected to electrophoresis under reducing or nonreducing conditions, as indicated. Lanes 1 through 6 contain (1) a covalent tetramer of Shaker subunits; (2) a covalent dimer of Shaker subunits; (3) Shaker-IR; (4) R362C single mutant; (5) F416C single mutant; and (6) R362C + F416C double mutant. A fluorograph of a representative experiment is shown (n = 5). Oocytes were treated with 5 mM NEM prior to disruption, except for cells expressing the covalent tetramer, which were treated with 0.1% H_2O_2 for 15 min at room temperature to oxidize intersubunit disulfide bonds between two cytoplasmic cysteine residues, C96 and C505, prior to NEM treatment (Schulteis et al., 1996). Under nonreducing conditions, the R362C + F416C protein comigrated with the disulfide-bonded circular tetramer (black arrow). The open arrow indicates the position of the linear tetramer under reducing conditions. The gray and black arrowheads denote the positions of the complex glycosylated dimeric and monomeric Shaker proteins, respectively (Nagaya and Papazian, 1997). The white arrowhead indicates the position of the immature, core-glycosylated form of the Shaker protein. All of the constructs matured efficiently, making the immature form virtually undetectable.

(C) After DTT treatment, normalized g-V curves were obtained in the absence (open symbols) or presence (black symbols) of Cd²⁺ for R362C + F416C channels. Values are shown as mean ± SEM, n = 4. Each data set was fitted with a single Boltzmann function (solid curves). The fitted parameters obtained in the absence of Cd²⁺ were $V_{1/2}$ = −28.2 ± 2.1 mV and slope = 14.3 ± 0.3 mV. The fitted parameters obtained in the presence of 10 μM Cd²⁺ were $V_{1/2}$ = 2.9 ± 1.2 mV and slope = 17.9 ± 2.1 mV.

(D) Oocytes expressing R362C + F416C channels were incubated in 2 mM DTT for 60–90 min and washed extensively. Current traces shown were recorded at +40 mV in the absence (black) or presence (gray) of Cd²⁺ and scaled to the same amplitude to compare activation kinetics.

(E) The time to half-maximal current amplitude ($t_{1/2}$) at +40 mV was measured in various concentrations of Cd²⁺, expressed as fold change in $t_{1/2}$, and plotted versus Cd²⁺ concentration. The data were fitted with a hyperbolic function (solid curve) with a half-maximal concentration of 1.7 ± 0.2 μM. Values are shown as mean ± SEM, n = 4–11.

A

B Control   1 μM Cd²⁺

C

D

Figure 8. Physical Proximity between R362 in S4 and A419 and F416 in Pore Domain Is Specific

(A) Shaker protein was metabolically labeled, isolated, and subjected to electrophoresis under reducing or nonreducing conditions, as indicated. Lanes 1 through 8 contain (1) a covalent tetramer of Shaker subunits; (2) Shaker-IR; (3) A417C single mutant; (4) R362C + A417C double mutant; (5) V453C single mutant; (6) R362C + V453C double mutant; (7) W454C single mutant; and (8) R362C + W454C double mutant. Oocytes were treated with 5 mM NEM prior to disruption, except for cells expressing the covalent tetramer, which were treated with 0.1% H_2O_2 for 15 min at room temperature to oxidize intersubunit disulfide bonds between two cytoplasmic cysteine residues, C96 and C505, prior to NEM treatment (Schulteis et al., 1996). The symbols are as follows: black arrow, disulfide-bonded circular tetramer under nonreducing conditions; open arrow, linear tetramer under reducing conditions; black arrowhead, complex glycosylated monomer; white arrowhead, immature core-glycosylated monomer. With the exception of R362C + A417C, the constructs matured efficiently.

(B–D) Oocytes expressing (B) R362C + A417C, (C) R362C + V453C, or (D) R362C + W454C were incubated in 2 mM DTT for 2 hr and washed extensively. Current traces were recorded in the absence (left panel) or presence (middle panel) of 1 μM Cd²⁺. The membrane potential was stepped from a holding potential of −100 mV to potentials between −60 and +90 mV in 10 mV increments. A representative experiment is shown (n = 4–7). Scale bars represent 2 μA and 40 ms. The right panel shows normalized g-V data obtained in the absence (open symbols) or presence (black symbols) of Cd²⁺. Values are

shown as mean ± SEM, n = 4–7. Each data set was fitted with a single Boltzmann function (solid curves), except for R362C + A417C, which did not reach a maximum conductance at +90 mV. Conductance values for R362C + A417C were normalized to the value obtained at +90 mV. Negative results were also obtained with the following double mutant constructs: I360C + V437C, I360C + V453C, I360C + I457C, L361C + V453C, L361C + W454C, L361C + V458C, R362C + V437C, R362C + G452C, V363C + A419C, R365C + V437C, R365C + V453C, R365C + W454C, R368C + V453C, and R368C + W454C (data not shown).

promoted by ion binding to adjacent sites have specific and distinct functional consequences.

In contrast, no intersubunit disulfide bonds were formed in R362C + A417C, R362C + V453C, or R362C + W454C. In addition, no evidence for high-affinity Cd²⁺ binding was obtained in these channels after DTT treatment. These negative results are highly significant because the KcsA structure predicts that A417, V453, and W454 are located at the periphery of the pore domain within 15 Å of F416 and A419 (Doyle et al., 1998). Specifically, the β carbon of A417 is expected to be located within 5 Å and 7.5 Å of the β carbons of F416 and A419, respectively, whereas the β carbons of V453 and W454 are expected to be located approximately 10 and 13 Å from that of F416. The MthK and KvAP structures, which are quite similar to KcsA in this region, make similar predictions (Jiang et al., 2002a, 2003a). Therefore, these results provide further evidence that formation of disulfide bonds between R362C and either F416C or A419C reflected specific physical proximity between these resi-

dues rather than the ability of a floppy voltage sensor to make promiscuous contacts with the pore domain. We also generated the R362C + E418C construct, but this protein was retained in the ER in an immature form, which suggests that it failed to fold properly (data not shown) (Papazian et al., 1995; Nagaya and Papazian, 1997; Tiwari-Woodruff et al., 1997).

Molecular Modeling of Voltage Sensor/Pore Interactions

We used a conformational search procedure based on molecular dynamics high temperature simulated annealing to generate a three-dimensional model of structural interactions between S4 and the pore domain in the activated conformation of Shaker channels (Roux, 2002). Initially, the modeling was performed using three constraints between S4 and the pore domain. First, based on our experimental results, we assumed that the β carbons of R362 in S4 and A419 in S5 are separated by less than 5 Å. Second, based on lanthanide resonance

energy transfer (LRET) measurements, we assumed that the distance from V363 in S4 to the center of symmetry in the pore is 22.5 Å (Cha et al., 1999). Third, we assumed that the distance between K380 at the cytoplasmic end of S4 and the nearest K390 at the cytoplasmic end of S5 is no longer than 10 Å, which is a reasonable maximum length for the intervening 9 residue S4–S5 linker in Shaker in an extended conformation. The Shaker pore domain, corresponding to segments S5, S6, and the P loop, was modeled in an open conformation according to the crystal structure of the calcium-activated MthK bacterial channel (Jiang et al., 2002a). Additional constraints deduced from a wide variety of experimental approaches were also incorporated into the conformational search procedure, including second site suppressor analysis in Shaker, identification of the ion binding site in the eag voltage sensor, distance measurements derived from tethered pore blockers, perturbation analysis of S1 through S4 and the pore domain, and channel dimensions as revealed by electron microscopy (Tiwari-Woodruff et al., 1997; Cha et al., 1999; Monks et al., 1999; Blaustein et al., 2000; Hong and Miller, 2000; Li-Smerin et al., 2000a, 2000b; Silverman et al., 2000; Tiwari-Woodruff et al., 2000; Sokolova et al., 2001; Silverman et al., 2003). Segments S1–S4 were assumed to be transmembrane α helices, in accordance with the results of perturbation analysis (Monks et al., 1999; Hong and Miller, 2000; Li-Smerin et al., 2000b).

Results of the modeling procedure placed the S4 segment in the groove formed at the interface between pore regions of adjacent subunits, nearly halfway between neighboring S5 helices. This was the only S4 position that simultaneously satisfied all the starting constraints. Inspection of this preliminary model revealed proximity between R377 in S4 and Y483 at the cytoplasmic end of S6. This was interesting because R377 and Y483 correspond to D540 and R665 in HERG (Figure 9A). Recently, functional evidence has been presented that D540 and R665 interact in HERG channels and that this interaction plays an important role in controlling channel gating (Tristani-Firouzi et al., 2002). Further refinement of the model with an additional constraint between S4 and the pore domain reflecting the HERG results, namely that R377 in S4 and Y483 in S6 are located within 5 Å of each other, did not significantly alter the position of S4 relative to the pore domain. The resulting three-dimensional model is shown in Figure 9, which highlights interactions between S4 and the pore, and Figure 10, which depicts the complete model. Interestingly, the S1–S4 helices in the model are packed in a counterclockwise fashion when viewed from the extracellular side of the membrane (Silverman et al., 2003), an arrangement similar to that seen in the X-ray structure of the isolated voltage sensor domain of KvAP (Jiang et al., 2003a).

In the model, interactions between R362 in S4 and A419 in S5 and between R377 in S4 and Y483 in S6 were simultaneously satisfied with the S4 segment as a straight, uninterrupted α helix of standard geometry. The assumption that S4 is helical is compatible with the structure of the KvAP voltage sensor (Jiang et al., 2003a). Our experimental results indicate that R362 in S4 is in proximity to the pore residues A419 and F416 in the adjacent subunit. It is therefore important to determine which S4 segment and pore domain belong to the same

subunit. During the conformational search procedure, the 9 residue linker between S4 and S5 (residues G381 through L389) was not included explicitly, and the S4 helix was not connected to any particular subunit. In the resulting model, K380, the carboxy-terminal residue in S4 (for modeling purposes), is 8 Å away from the nearest K390, the amino-terminal residue in S5 (for modeling purposes). The distance between K380 and K390 from each of the other monomers is 29, 37, and 46 Å. Because the short S4–S5 linker in Shaker would not suffice to connect the carboxyl terminus of S4 to the amino terminus of S5 over such large distances, S4 can be linked to S5 and S6 as a continuous polypeptide in only one way. This result unambiguously predicts the boundaries of a single subunit, as shown in Figure 9D. In the three-dimensional model of the open channel conformation, R362 in S4 in one subunit is within atomic proximity of A419 in S5 in the adjacent subunit located in the clockwise direction as seen from the extracellular side of the membrane.

A Single Structural Model Is Compatible with a Large Variety of Experimental Data

The three-dimensional model of voltage sensor-pore interactions that we have generated is compatible with experimental constraints on the structure of voltage-dependent K^+ channels derived from a wide variety of approaches (Roux, 2002). In particular, the position of S4 in the model is consistent with distance estimates made with tethered quaternary ammonium blockers (Blaustein et al., 2000) and intersubunit distances estimated from LRET measurements (Cha et al., 1999). The experimentally estimated distance between V363C located on opposite sides of the tetramer is 45 Å, while the corresponding distance in the model is 43 Å, using the β carbon atom as the reference point. Since the absolute accuracy of the donor-acceptor distance in LRET is approximately 12% (Getz et al., 1998; Selvin, 2002), this distance constraint can only be satisfied if S4 is located roughly in the groove between pore domains from adjacent subunits (Roux, 2002). Furthermore, the location of S4 appears to be compatible with electrostatic calculations of Elinder and coworkers (2001). Based on the effect of a charged residue at 362 on the reaction rate of E418C with methanethiosulfonate reagents, they estimated that R362 moves to within 8 Å of 418 during activation and C-type inactivation. In our model, the distance between the Cβ atoms of R362 and E418 is 11 Å. In contrast, it is difficult to reconcile many of these experimental findings with the KvAP X-ray structure (Jiang et al., 2003a) or with models of the open and closed channel conformations proposed by Jiang et al. (2003b).

The Shaker pore domain, corresponding to segments S5, S6, and the P loop, was modeled in an open conformation according to the crystal structure of the calcium-activated MthK bacterial channel (Jiang et al., 2002a, 2002b). Use of the open channel structure was particularly appropriate because the S4/pore interactions that we have identified occur in an activated conformation. Although some data suggest that the structure of the open conformation in Shaker diverges from that of MthK near the intracellular vestibule (Liu et al., 1997; del Camino et al., 2000), the MthK structure is likely to provide

Figure 9. A Model of Voltage Sensor-Pore Interactions in the Activated Conformation of Shaker Channels Is Shown

(A) A side view of the model showing S4 and the pore domain. The S4 segment, corresponding to residues K350 to K380, was assumed to be an α helix (shown in blue). The central pore domain, corresponding to residues K390 to D490, was modeled according to the MthK structure (Jiang et al., 2002a). S5 is shown in yellow, S6 in green, and the pore helices and selectivity filter in gray. The red spheres represent the Cβ atoms of R362 and A419, whereas the orange spheres represent the Cβ atoms of R377 and Y483. The blue-yellow arrow indicates the connection between the S4 and S5 helices from the same subunit, as predicted by the model. At the bottom is shown an alignment of the S4 and S6 sequences from Shaker and HERG. Identical residues are shown in bold. Asterisks denote the positions of D540 and R665 in the HERG sequence (Tristani-Firouzi et al., 2002).
(B) The model is viewed from an intracellular perspective.
(C) The model is viewed from an extracellular perspective.
(D) A side view of the model, in which S4 and the pore domain from each of the four subunits are shown in different colors to illustrate intersubunit interactions.
(E) A view from an extracellular perspective, in which S4 and the pore domain from each of the four subunits are shown in different colors to illustrate intersubunit interactions. R362 from one subunit is predicted to interact with A419 in the neighboring monomer located in the clockwise direction, as seen from the extracellular side of the membrane.
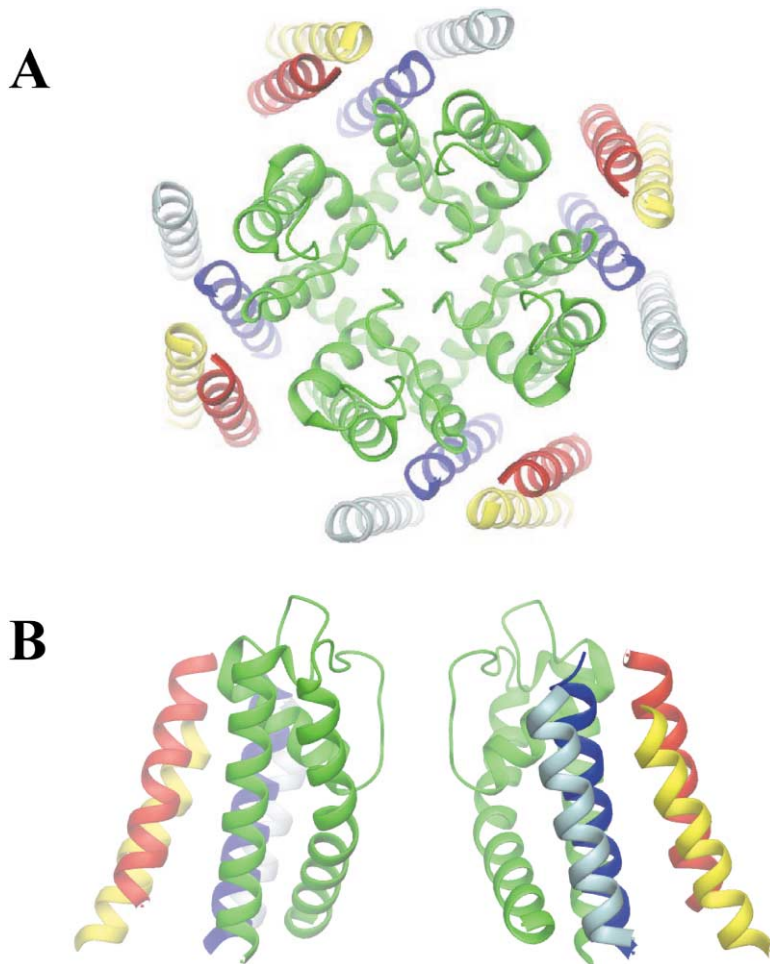
A

B

Figure 10. Complete Model of Shaker Transmembrane Region, Including S1–S4 and the Pore Domain, Is Shown

(A) The model is viewed from an extracellular perspective.

(B) A side view is shown. Two subunits have been removed for clarity. The color code is as follows: pore domain, green; S1, light blue-gray; S2, yellow; S3, red; S4, blue.

a good model for the Shaker pore for several reasons. First, there is a high degree of sequence homology between KcsA, MthK, KvAP, and the pore-forming region of Shaker (Doyle et al., 1998; Jiang et al., 2002a, 2003a). Second, structures of the pore in KcsA, MthK, and KvAP share significant similarity, confirming that the structures of K$^+$-selective pores are highly conserved (Doyle et al., 1998; Jiang et al., 2002a, 2003a). Third, direct evidence for structural similarity between Shaker and KcsA has been obtained from toxin binding (MacKinnon et al., 1998). Finally, chimeras between the Shaker voltage sensor and the KcsA pore form voltage-gated, K$^+$-selective channels, indicating that these modules are structurally compatible (Lu et al., 2001, 2002).

Use of the MthK X-ray structure to build a homology model for the Shaker pore domain was essential for defining the topology of the polypeptide chain. The open channel has a wide intracellular vestibule where the amino termini (K390) of S5 segments from adjacent subunits are separated by approximately 33 Å, which helps considerably to establish the boundaries of an individual subunit. In contrast, it was not possible to resolve the topology of the subunit using a three-dimensional model corresponding to the closed state, constructed on the basis of the X-ray structure of the closed KcsA channel where the separation between the amino-terminal ends of adjacent S5 segments is only 17 Å (Roux, 2002).

A voltage sensor/pore interaction surface was previously proposed on the basis of perturbation analysis. Tryptophan scanning analysis of the pore domain in Shaker channels revealed that mutations with a high impact on the position of the g-V curve clustered at the surface of the S5–S6 domain near the subunit interface (Li-Smerin et al., 2000a). The high-impact residues formed a stripe tilted at an angle of about +45°. In contrast, our model suggests that the S4 segment is tilted at an angle of approximately −15° in the activated conformation. More recently, the tryptophan mutants have been analyzed for their effects on the gating charge-voltage (q-V) curve (K.J. Swartz, personal communication). Because the q-V curve reflects movement of the voltage sensor rather than opening of the pore, this may be more pertinent for defining residues in the pore that directly contact the voltage sensor. Significantly, many of the high-impact residues defined by perturbations in the q-V curve lie directly underneath the position of S4 in our model (K.J. Swartz, personal communication). Thus, the high-impact mutations defined by their effect on the q-V curve may identify an interaction surface between the pore and the S4 segment per se.

In summary, we have presented evidence that S4 in the voltage sensor interacts directly with the pore domain in K$^+$ channels and identified residues that move into atomic proximity of each other during activation. We

have generated a three-dimensional model of voltage sensor-pore interactions in Shaker channels that predicts that the S4 segment spans the groove between pore domains contributed by adjacent subunits and that, in the activated conformation, the amino-terminal end of S4 is in proximity to the pore domain of the subunit located in the clockwise direction when viewed from an extracellular perspective.

Experimental Procedures

Mutagenesis and Expression

Mutations were generated by PCR, using a three or four primer strategy (Landt et al., 1990; Sarkar and Sommer, 1990). PCR products were digested with appropriate restriction enzymes and transferred into a Bluescript (Stratagene Inc.) subclone of the Shaker-IR cDNA. Transferred regions were verified by sequencing. All constructs contained the IR deletion of amino acids 6–46 to remove N-type inactivation (Hoshi et al., 1990). Run-off transcripts of RNA were prepared and injected into *Xenopus* oocytes as previously described (Santacruz-Toloza et al., 1994; Papazian et al., 1995). Injected oocytes were stored at 18°C for 1–2 days in ND96 (96 mM NaCl, 5 mM KCl, 1 mM MgCl$_2$, 1.8 mM CaCl$_2$, 5 mM HEPES [pH 7.5]) prior to electrophysiological analysis.

The covalent tetramer of Shaker subunits was kindly provided by Dr. Fred Sigworth and has been previously described (Schulteis et al., 1996). Covalent dimers of Shaker-IR subunits were engineered according to Heginbotham and MacKinnon (1992).

Electrophysiology

Whole-cell currents were recorded using a two-electrode voltage clamp (OC-725; Warner Electronics). Recording electrodes were filled with 3 M KCl and had resistances of 0.3–1 MΩ. Currents were recorded at room temperature (20°C–22°C) in modified Barth's saline solution (1 mM KCl, 88 mM NaCl, 2.4 mM NaHCO$_3$, 0.82 mM MgSO$_4$, 0.33 mM Ca(NO$_3$)$_2$, 0.41 mM CaCl$_2$, 10 mM HEPES [pH 7.5]). The bath solution also contained CdCl$_2$, ZnSO$_4$, or DTT, as noted. Oocytes were incubated at room temperature for various times up to 2 hr in ND96 containing 2 mM DTT and washed extensively prior to recording. The bath solution was changed using a gravity-driven perfusion system that was governed by solenoid valves and controlled manually. Linear leak and capacitive currents were subtracted using a P/-4 protocol. Data were acquired using pCLAMP v. 5.5.1 (Axon Instruments, Inc.) and filtered at 1–4 kHz.

Currents were recorded by depolarizing from a holding potential of −100 mV to voltages from −100 to +60 mV in 10 or 20 mV increments. Conductance values (g), obtained from steady-state current amplitudes at various voltages, were calculated according to g = (I/V − V$_{rev}$). The reversal potential was estimated to be −75 mV for a bath solution containing 1 mM KCl. Conductance values were normalized to the maximal conductance value (g$_{max}$) obtained under control conditions in the same oocyte. Normalized conductance values were plotted versus voltage, and the data were fitted using a single, first-power Boltzmann equation to obtain the midpoint potential and slope factor. The time to half-maximal current amplitude was measured to obtain a value for t$_{1/2}$ as previously described (Silverman et al., 2000).

Data are provided as mean ± SEM. Statistical significance was assessed using a one-way ANOVA as indicated.

Biochemistry

For biochemical analysis, RNA was coinjected with 400 nCi per oocyte of in vitro translation grade [^{35}S]methionine (Santacruz-Toloza et al., 1994). Oocytes (n = 40–60) were harvested 44–48 hr after injection. Oocytes were incubated for 15 min in the presence of 5 mM NEM to protect free sulfhydryl groups. Shaker proteins were solubilized, immunoprecipitated, and subjected to electrophoresis under either reducing (10% 2-mercaptoethanol) or nonreducing (16 mM iodoacetamide) conditions on 5%–15% gradient gels with 3% stacking gels (Schulteis et al., 1996). Gels were soaked in autoradiographic enhancer, dried, and exposed to film.

Molecular Modeling

Molecular dynamics calculations were performed essentially as described previously (Roux, 2002). A variety of experimental results were incorporated in the modeling as artificial energy restraints. In addition to the S1 (A226–E247), S2 (F279–A300), S3 (V311–A332), and S4 (K350–K380) transmembrane segments (modeled as α helices), the S5–S6 pore domain of Shaker including residues K390 to D490 was constructed on the basis of the MthK structure (Jiang et al., 2002a).

References

Alberts, I.L., Nadassy, K., and Wodak, S.J. (1998). Analysis of zinc binding sites in protein crystal structures. Protein Sci. *7*, 1700–1716.

Aggarwal, S.K., and MacKinnon, R. (1996). Contribution of the S4 segment to gating charge in the Shaker K$^+$ channel. Neuron *16*, 1169–1177.

Baukrowitz, T., and Yellen, G. (1995). Modulation of K$^+$ current by frequency and external K$^+$: a tale of two inactivation mechanisms. Neuron *15*, 951–960.

Bernèche, S., and Roux, B. (2000). Molecular dynamics of the KcsA K$^+$ channel in a bilayer membrane. Biophys. J. *78*, 2900–2917.

Bezanilla, F. (2000). The voltage sensor in voltage-dependent ion channels. Physiol. Rev. *80*, 555–592.

Bezanilla, F. (2002). Voltage sensor movements. J. Gen. Physiol. *120*, 465–473.

Bezanilla, F., Perozo, E., and Stefani, E. (1994). Gating of Shaker K$^+$ channels: II. The components of gating currents and a model of channel activation. Biophys. J. *66*, 1011–1021.

Blaustein, R.O., Cole, P.A., Williams, C., and Miller, C. (2000). Tethered blockers as molecular 'tape measures' for a voltage-gated K$^+$ channel. Nat. Struct. Biol. *7*, 309–311.

Careaga, C.L., and Falke, J.J. (1992). Thermal motions of surface alpha-helices in the D-galactose chemosensory receptor. Detection by disulfide trapping. J. Mol. Biol. *226*, 1219–1235.

Castagnetto, J.M., Hennessy, S.W., Roberts, V.A., Getzoff, E.D., Tainer, J.A., and Pique, M.E. (2002). MDB: the metalloprotein database and browser at the Scripps Research Institute. Nuc. Acids Res. *30*, 379–382. (http://metallo.scripps.edu)

Cha, A., Snyder, G.E., Selvin, P.R., and Bezanilla, F. (1999). Atomic scale movement of the voltage-sensing region in a potassium channel measured via spectroscopy. Nature *402*, 809–813.

Choi, K.L., Aldrich, R.W., and Yellen, G. (1991). Tetraethylammonium blockade distinguishes between two inactivation mechanisms in voltage-activated K$^+$ channels. Proc. Natl. Acad. Sci. USA *88*, 5092–5095.

del Camino, D., Holmgren, M., Liu, Y., and Yellen, G. (2000). Blocker protection in the pore of a voltage-gated K$^+$ channel and its structural implications. Nature *403*, 321–325.

Doyle, D.A., Morais Cabral, J., Pfuetzner, R.A., Kuo, A., Gulbis, J.M., Cohen, S.L., Chait, B.T., and MacKinnon, R. (1998). The structure of the potassium channel: molecular basis of K$^+$ conduction and selectivity. Science *280*, 69–77.

Elinder, F., Mannikko, R., and Larsson, H.P. (2001). S4 charges move

close to residues in the pore domain during activation in a K⁺ channel. J. Gen. Physiol. *118*, 1–10.

Gandhi, C.S., and Isacoff, E.Y. (2002). Molecular models of voltage sensing. J. Gen. Physiol. *120*, 455–463.

Getz, E.B., Cooke, R., and Selvin, P.R. (1998). Luminescence resonance energy transfer measurements in myosin. Biophys. J. *74*, 2451–2458.

Harding, M.M. (2001). Geometry of metal-ligand interactions in proteins. Acta Crystallogr. D *57*, 401–411.

Heginbotham, L., and MacKinnon, R. (1992). The aromatic binding site for tetraethylammonium ion on potassium channels. Neuron *8*, 483–491.

Heginbotham, L., Abramson, T., and MacKinnon, R. (1992). A functional connection between the pores of distantly related ion channels as revealed by mutant K⁺ channels. Science *258*, 1152–1155.

Holmgren, M., Shin, K.S., and Yellen, G. (1998). The activation gate of a voltage-gated K⁺ channel can be trapped in the open state by an intersubunit metal bridge. Neuron *21*, 617–621.

Hong, K.H., and Miller, C. (2000). The lipid-protein interface of a Shaker K⁺ channel. J. Gen. Physiol. *115*, 51–58.

Horn, R. (2002). Coupled movements in voltage-gated ion channels. J. Gen. Physiol. *120*, 449–453.

Hoshi, T., Zagotta, W.N., and Aldrich, R.W. (1990). Biophysical and molecular mechanisms of Shaker potassium channel inactivation. Science *250*, 533–538.

Jiang, Y., Lee, A., Chen, J., Cadene, M., Chait, B.T., and MacKinnon, R. (2002a). Crystal structure and mechanism of a calcium-gated potassium channel. Nature *417*, 515–522.

Jiang, Y., Lee, A., Chen, J., Cadene, M., Chait, B.T., and MacKinnon, R. (2002b). The open pore conformation of potassium channels. Nature *417*, 523–526.

Jiang, Y., Lee, A., Chen, J., Ruta, V., Cadene, M., Chait, B.T., and MacKinnon, R. (2003a). X-ray structure of a voltage-dependent K⁺ channel. Nature *423*, 33–41.

Jiang, Y., Ruta, V., Chen, J., Lee, A., and MacKinnon, R. (2003b). The principle of gating charge movement in a voltage-dependent K⁺ channel. Nature *423*, 42–48.

Jung, K., Voss, J., He, M., Hubbell, W.L., and Kaback, H.R. (1995). Engineering a metal binding site within a polytopic membrane protein, the lactose permease of *Escherichia coli*. Biochemistry *34*, 6272–6277.

Keifer, L.L., and Fierke, C.A. (1994). Functional characterization of human carbonic anhydrase II variants with altered zinc binding sites. Biochemistry *33*, 15233–15240.

Landt, O., Grunert, H.P., and Hahn, U. (1990). A general method for rapid site-directed mutagenesis using the polymerase chain reaction. Gene *96*, 125–128.

Larsson, H.P., Baker, O.S., Dhillon, D.S., and Isacoff, E.Y. (1996). Transmembrane movement of the Shaker K⁺ channel S4. Neuron *16*, 387–397.

Ledwell, J.L., and Aldrich, R.W. (1999). Mutations in the S4 region isolate the final voltage-dependent cooperative step in potassium channel activation. J. Gen. Physiol. *113*, 389–414.

Li-Smerin, Y., Hackos, D.H., and Swartz, K.J. (2000a). A localized interaction surface for voltage-sensing domains on the pore domain of a K⁺ channel. Neuron *25*, 411–423.

Li-Smerin, Y., Hackos, D.H., and Swartz, K.J. (2000b). Alpha-helical structural elements within the voltage-sensing domains of a K⁺ channel. J. Gen. Physiol. *115*, 33–50.

Liu, Y., Holmgren, M., Jurman, M.E., and Yellen, G. (1997). Gated access to the pore of a voltage-dependent K⁺ channel. Neuron *19*, 175–184.

Loland, C.J., Norregaard, L., and Gether, U. (1999). Defining proximity relationships in the tertiary structure of the dopamine transporter. J. Biol. Chem. *274*, 36928–36934.

Loussouarn, G., Phillips, L.R., Masia, R., Rose, T., and Nichols, C.G. (2001). Flexibility of the Kir6.2 inward rectifier K⁺ channel pore. Proc. Natl. Acad. Sci. USA *98*, 4227–4232.

Lu, Z., Klem, A.M., and Ramu, Y. (2001). Ion conduction pore is conserved among potassium channels. Nature *413*, 809–813.

Lu, Z., Klem, A.M., and Ramu, Y. (2002). Coupling between voltage sensors and activation gate in voltage-gated K⁺ channels. J. Gen. Physiol. *120*, 663–676.

MacAulay, N., Bendahan, A., Loland, C.J., Zeuthen, T., Kanner, B.I., and Gether, U. (2001). Engineered Zn²⁺ switches in the gamma-amino butyric acid (GABA) transporter-1. Differential effects on GABA uptake and currents. J. Biol. Chem. *276*, 40476–40485.

MacKinnon, R. (1991). Determination of the subunit stoichiometry of a voltage-activated potassium channel. Nature *350*, 232–235.

MacKinnon, R., and Yellen, G. (1990). Mutations affecting TEA blockade and ion permeation in voltage-activated K⁺ channels. Science *250*, 276–279.

MacKinnon, R., Cohen, S.L., Kuo, A., Lee, A., and Chait, B.T. (1998). Structural conservation in prokaryotic and eukaryotic potassium channels. Science *280*, 106–109.

Monks, S.A., Needleman, D.J., and Miller, C. (1999). Helical structure and packing orientation of the S2 segment in the Shaker K⁺ channel. J. Gen. Physiol. *113*, 415–423.

Nagaya, N., and Papazian, D.M. (1997). Potassium channel α and β subunits assemble in the endoplasmic reticulum. J. Biol. Chem. *272*, 3022–3027.

Norregaard, L., Visiers, I., Loland, C.J., Ballesteros, J., Weinstein, H., and Gether, U. (2000). Structural probing of a microdomain in the dopamine transporter by engineering of artificial Zn²⁺ binding sites. Biochemistry *39*, 15836–15846.

Papazian, D.M., Shao, X.M., Seoh, S.-A., Mock, A.F., Huang, Y., and Wainstock, D.H. (1995). Electrostatic interactions of S4 voltage sensor in Shaker K⁺ channel. Neuron *14*, 1293–1301.

Roux, B. (2002). What can be deduced about the structure of Shaker from available data? Novartis Found. Symp. *245*, 84–101.

Ruta, V., Jiang, Y., Lee, A., Chen, J., and MacKinnon, R. (2003). Functional analysis of an archaebacterial voltage-dependent K⁺ channel. Nature *422*, 180–185.

Santacruz-Toloza, L., Huang, Y., John, S.A., and Papazian, D.M. (1994). Glycosylation of Shaker potassium channel protein in insect cell culture and in *Xenopus* oocytes. Biochemistry *33*, 5607–5613.

Sarkar, G., and Sommer, S.S. (1990). The "megaprimer" method of site-directed mutagenesis. Biotechniques *8*, 404–407.

Schulteis, C.T., Nagaya, N., and Papazian, D.M. (1996). Intersubunit interaction between amino- and carboxyl-terminal cysteine residues in tetrameric Shaker K⁺ channels. Biochemistry *35*, 12133–12140.

Schulteis, C.T., Nagaya, N., and Papazian, D.M. (1998). Subunit folding and assembly steps are interspersed during Shaker potassium channel biogenesis. J. Biol. Chem. *273*, 26210–26217.

Schoppa, N.E., and Sigworth, F.J. (1998). Activation of Shaker potassium channels. III. An activation gating model for wild-type and V2 mutant channels. J. Gen. Physiol. *111*, 313–342.

Selvin, P.R. (2002). Principles and biophysical applications of lanthanide-based probes. Annu. Rev. Biophys. Biomol. Struct. *31*, 275–302.

Seoh, S.-A., Sigg, D., Papazian, D.M., and Bezanilla, F. (1996). Voltage-sensing residues in the S2 and S4 segments of the Shaker K⁺ channel. Neuron *16*, 1159–1167.

Silverman, W.R., Tang, C.-Y., Mock, A.F., Huh, K.-B., and Papazian, D.M. (2000). Mg²⁺ modulates voltage-dependent activation in ether-à-go-go potassium channels by binding between transmembrane segments S2 and S3. J. Gen. Physiol. *116*, 663–678.

Silverman, W.R., Roux, B., and Papazian, D.M. (2003). Structural basis of two-stage voltage-dependent activation in K⁺ channels. Proc. Natl. Acad. Sci. USA *100*, 2935–2940.

Sokolova, O., Kolmakova-Partensky, L., and Grigorieff, N. (2001). Three-dimensional structure of a voltage-gated potassium channel at 2.5 nm resolution. Structure *9*, 215–220.

Starace, D.M., and Bezanilla, F. (2001). Histidine scanning mutagenesis of basic residues of the S4 segment of the Shaker K⁺ channel. J. Gen. Physiol. *117*, 469–490.

Starace, D.M., Stefani, E., and Bezanilla, F. (1997). Voltage-dependent proton transport by the voltage sensor of the Shaker K$^+$ channel. Neuron *19*, 1319–1327.

Tiwari-Woodruff, S.K., Schulteis, C.T., Mock, A.F., and Papazian, D.M. (1997). Electrostatic interactions between transmembrane segments mediate folding of Shaker potassium channel subunits. Biophys. J. *72*, 1489–1500.

Tiwari-Woodruff, S.K., Lin, M.A., Schulteis, C.T., and Papazian, D.M. (2000). Voltage-dependent structural interactions in the Shaker K$^+$ channel. J. Gen. Physiol. *115*, 123–138.

Tristani-Firouzi, M., Chen, J., and Sanguinetti, M.C. (2002). Interactions between S4–S5 linker and S6 transmembrane domain modulate gating of HERG K$^+$ channels. J. Biol. Chem. *277*, 18994–19000.

Yamagishi, T., Janecki, M., Marban, E., and Tomaselli, G.F. (1997). Topology of the P segments in the sodium channel pore revealed by cysteine mutagenesis. Biophys. J. *73*, 195–204.

Yellen, G., Jurman, M.E., Abramson, T., and MacKinnon, R. (1991). Mutations affecting internal TEA blockade identify the probable pore-forming region of a K$^+$ channel. Science *251*, 939–942.

Yellen, G., Sodickson, D., Chen, T.-Y., and Jurman, M.E. (1994). An engineered cysteine in the external mouth of a K$^+$ channel allows inactivation to be modulated by metal binding. Biophys. J. *66*, 1068–1075.

Yifrach, O., and MacKinnon, R. (2002). Energetics of pore opening in a voltage-gated K$^+$ channel. Cell *111*, 231–239.

Yusaf, S.P., Wray, D., and Sivaprasadarao, A. (1996). Measurement of the movement of the S4 segment during activation of a voltage-gated potassium channel. Pflüg. Arch. *433*, 91–97.

Zagotta, W.N., Hoshi, T., and Aldrich, R.W. (1994). Shaker potassium channel gating. III: Evaluation of kinetic models for activation. J. Gen. Physiol. *103*, 321–362.